MATERIALE PLASTICE
https://revmaterialeplastice.ro
https://doi.org/10.37358/Mat.Plast.1964

Mechanical Properties and Failure Behavior of Epoxy Rubber Powder Composites Reinforced with Hollow Beads

WU ZHE, ZHANG ZHEN, ZHANG XINLONG*, JIANG HAIFENG, ZHANG ZHONGCHI
College of Mechanical and Electrical Engineering Northeast Forestry University Harbin 150040, P.O. Box 3010, No. 26, He Xing Road, China

***Abstract**: In this paper, new epoxy resin/rubber powder/hollow beads three-phase composites were prepared by designing the incorporation of fly ash hollow beads with different mass fractions (5%, 10%, 15%, and 20%) as new reinforcing phases into epoxy resin/rubber powder two-phase composites with 5% mass fraction of carbon black rubber powder. Quasi-static compression tests were conducted at room temperature to test the compressive properties of the oxygen resin/rubber powder/hollow beads composites. Calculate the energy absorption properties and energy absorption efficiency of the composites from the compression curves. Fracture characteristics of compressed material specimens with microscopic morphology were observed by scanning electron microscopy. By systematically analyzing the effect of fly ash hollow beads content on the mechanical properties of epoxy resin/rubber powder/hollow beads three-phase composites, it was found that fly ash hollow beads as reinforcing materials can effectively improve the brittleness and yield strength of epoxy resin/rubber powder as well as the energy-absorbing properties and efficiency of the composites. The energy absorption properties of the epoxy resin/rubber powder/hollow beads composites increased and then decreased with the increase in the mass fraction of fly ash hollow beads. In the epoxy resin/rubber powder/hollow beads composites, the most significant performance was observed when the mass fraction of fly ash was 10%.*

***Keywords**: composite, hollow microbeads, epoxy, carbon powder, compression, energy absorption*

1. Introduction

As one of the three recognized general-purpose thermosetting resins, epoxy resin has an internal mesh cross-linking structure, which gives it excellent mechanical properties, good chemical stability and durability [1-3]. Therefore, it is widely used in the fields of electronic packaging, automotive, aerospace and so on [4-8]. However, due to its highly cross-linked structure, epoxy resin has low toughness and poor impact and cracking resistance, which limits its application as a structural material [9-13]. In recent years, the research on the reinforcement and modification of epoxy resin has gradually been emphasized, and new composite materials with epoxy resin as the matrix phase have been widely used in various fields [14-16].

Supplements are often added to improve their physical, chemical and mechanical properties. These additives usually include modified fibers and granular materials [17-19]. It was shown that jute reinforced composites have good tensile and flexural properties, while banana fiber and coconut fiber reinforced materials contribute to impact resistance and energy absorption properties are improved to some extent [20]. Particulates such as alumina, silicon carbide, rubber powder, and silicon oxide can be used as reinforcement materials in composites. The use of these particles can significantly improve the overall mechanical properties of composites compared to pure epoxy resins [21, 22]. However, researchers have found that the addition of just a single fiber and particulate material is limited in enhancing the mechanical properties of epoxy resins. Therefore, in order to further improve the energy-absorbing properties of composites, more and more scholars have begun to study the incorporation of a third supplementary reinforcing filler into the composites [23-25]. Yang et al. used polyaniline with fine particle structure as an interfacial reinforcing agent to enhance the interfacial adhesion of p-phenylene benzobisoxazole fiber/epoxy composites. The results showed that the addition of particles increased the interfacial shear strength and interlaminar shear strength of p-phenylene benzobisoxazole fiber / epoxy

*email; zhangxinlong@nefu.edu.cn

composites by 60.16 and 54.83%, respectively [26]. Sarmin et al. doped chitosan powder into epoxy resin/date palm fiber composites and the results of the study showed that the thermal stability of epoxy resin/date palm fiber composites was improved [27]. Researchers Perumal et al. showed that the incorporation of zircon particles with a mass fraction of 10% into a glass fiber epoxy composite resulted in an increase in the tensile strength, tensile modulus, flexural strength and flexural modulus of the composite by 33.33%, 12.56%, 32.88%, and 15.74%, respectively [28]. However, from the current research situation, most of the scholars in the study of reinforced epoxy composites, the selected reinforcing materials are focused on the mechanical properties of flexural, shear and tensile, while the research on the improvement of energy-absorbing properties of the composites is relatively less [29, 30]. Therefore, in order to further enhance the energy-absorbing properties of the composites, a more suitable reinforcing material needs to be selected. In this paper, fly ash hollow beads are used as reinforcing materials to be incorporated into rubber powder epoxy composites. Fly ash hollow beads are a kind of hollow microspherical industrial waste made of aluminum silicate with good dispersion, homogeneity, inertness and chemical stability. The special properties of the hollow structure include lightness, rigidity and compression resistance, as well as strength, which makes it an ideal reinforcing material that can be added to composites to enhance their properties. The application of this reinforcing material can realize two purposes: on the one hand, it can reduce the density of the composite material and lower the weight; on the other hand, it can improve the mechanical properties and energy-absorbing properties of the composite material [31, 32]. However, there are few studies on the reinforcement of fly ash hollow beads in rubber powder epoxy composites. Therefore, it is of research value to study the application and enhancement of fly ash hollow beads in rubber powder epoxy resin composites.

Based on the previous research of our group, it was shown that carbon black rubber powder epoxy resin composites with a mass fraction of 5% showed the best mechanical properties [33], so in this study, fly ash hollow beads were used to toughen the rubber powder epoxy resin matrix with a mass fraction of 5%. Quasi-static compression tests were carried out using a universal testing machine to obtain stress-strain curves, focusing on the compression characteristics of the specimens. The mechanical evolution process and energy-absorbing properties of the microbead rubber powder epoxy resin were analyzed by combining the scanning electron microscope pictures and the macroscopic changes of the specimens.

2. Materials and methods

2.1. Experimental materials

The bisphenol A epoxy resin used in the experiment was E51 epoxy resin produced by Yueyang Baling Petrochemical Co. N220 carbon black rubber powder was purchased from North China Fine Chemical Co, the specific parameters are shown in Table 1. Fly ash hollow beads were purchased from Hebei Jingjia Mineral Products Processing Co, the specific parameters are shown in Table 2. Coupling agent KH-550 was purchased from Changzhou Runxiang Chemical Co. All the above materials are industrial grade materials without further purification.

Table 1. Physical and chemical properties of carbon black rubber powder

Particle diameter **(mm)**	Density（**g/L**）	Individual particle strength **(CN)**	300% Constant stretch pressure **(MPa)**
0.178±0.005	180±20	≤50	-1.9±1.0

Table 2. Physical and chemical properties of fly ash hollow beads

Packing density **(g/cm^3)**	True Density **(g/cm^3)**	Particle diameter **(μm)**	compressive strength **(MPa)**
0.3 ~ 0.6	1.2 ~ 1.4	20 ~ 400	10 ~ 50

2.2. Experimental equipment

The universal testing machine used in the test is WDW-100, which is produced in Changchun Kexin company. The scanning electron microscope adopts the EM-30Plus model produced by COEXM company. The DZF vacuum drying oven is produced by Shanghai Yiheng Technology Instrument Co., Ltd. and DF-101 heat collecting magnetic mixer is purchased from Gongyi Kerui Instrument Co., Ltd.

2.3. Experimental method

This study used a silane coupling agent (KH550) to modify the surface of carbon black rubber powder and fly ash hollow microbeads for 20s, and then added into epoxy resin. The modified carbon black rubber powder and fly ash hollow microbeads were fully dried and then fully mechanically stirred in a magnetic stirrer at different mass fractions. After eliminating air bubbles in a vacuum drying oven, the liquid epoxy/rubber powder/hollow bead mixture was injected into the mold. After 48 h at room temperature, samples with dimensions of 10 mm × 10 mm × 25 mm were demolded as shown in Figure 1. Compression tests were carried out on specimens with different mass fractions using a WDW universal testing machine. The compression tests were carried out at a strain rate of 10^{-2} s^{-1}. After spraying gold on the fracture surface of the compression specimens, the microscopic morphology of the specimens was observed under a scanning electron microscope.

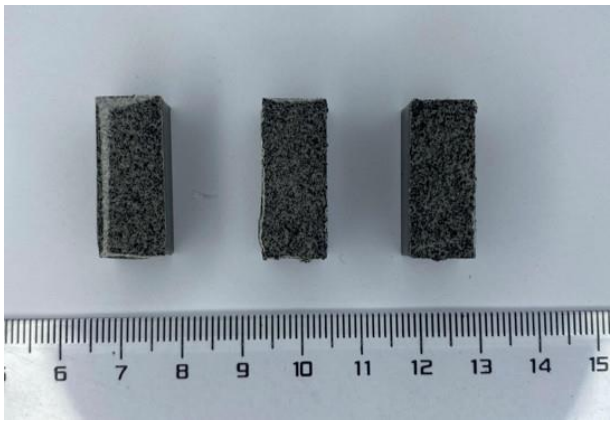

Figure 1. Composite material specimens

3. Results and discussions

3.1. Density analysis of materials

In order to minimize the effect of chance error during the overall quasi-static compression experiments, groups of 10 specimens each were prepared for fly ash hollow beads with mass fractions of 5%, 10%, 15%, and 20%. For epoxy resin/rubber powder/hollow beads three-phase composites the theoretical density can be calculated using the following equation:

$$\rho_c = \rho_E(1 - V_n - V_H) + \rho_n V_n + \rho_H V_H \quad (1)$$

In equation 1, ρ_c is the theoretical density of epoxy resin/N220 carbon black rubber powder/hollow beads composite, V_n is the volume fraction of N220 carbon black rubber powder, ρ_E is the density of pure epoxy resin, ρ_n is the density of N220 carbon black rubber powder, ρ_H is the density of hollow beads of fly ash, and V_H is the volume fraction of hollow beads of fly ash. The volume fraction V_H of the fly ash hollow beads can be calculated from the density of the fly ash hollow beads and its mass fraction in the epoxy resin/rubber powder/hollow beads three-phase composite:

$$V_H = \frac{\omega_H}{\omega_H + \frac{(1 - \omega_H - 0.05)\rho_H}{\rho_E} + \frac{0.05\rho_H}{\rho_n}} \quad (2)$$

Table 3 shows the volume fractions corresponding to different mass fractions of fly ash hollow beads and the theoretical and actual densities of the epoxy resin/rubber powder/hollow beads three-phase composites calculated according to equation 2 above. It can be seen that, due to the density of fly ash hollow beads being less than the density of epoxy resin, when the mass fraction of N220 carbon black rubber powder is 5% and the volume fraction is 25.3%, with the increase of the mass fraction of fly ash hollow beads, the volume fraction of fly ash hollow beads are also increasing, and the growth rate of the volume fraction exceeds the growth rate of the mass fraction, and the theoretical and actual density of three-phase composites both decreased.

Table 3. Density and volume fraction of composites with different mass fractions of hollow beads

Mass fraction of hollow beads（ω_H/%）	Volume fraction of hollow beads（V_H/%）	Theoretical density of composite materials（ρ_c/g·cm^{-3}）	Actual density of composites（ρ_a/g·cm^{-3}）
5	9.54	0.844	0.826
10	18.02	0.784	0.756
15	25.62	0.730	0.695
20	32.47	0.682	0.643

3.2 Mechanical properties analysis of composite materials

Figure 2 shows the macroscopic state of the epoxy resin/rubber powder/hollow beads three-phase composite specimens under different strains in the quasi-static compression experiments. According to the macroscopic deformation diagrams under different strains, it can be seen that the epoxy resin/rubber powder/hollow beads three-phase composite specimens have just passed through the linear elasticity stage, and the slight deformation occurs when the strain is 10%, and the deformation is very slight. As shown in Figure 2b, the surface of the three-phase composite material is compressed, and a "grid-like" pattern appears, with a slight axial deformation in the surrounding direction, and a tendency to spread in all directions. When the strain reaches 20%, as shown in Figure 2c, the three-phase composite material specimen is on both sides of the obvious "bulging" deformation. As the strain continues to increase to 30%, the "bulge" of the epoxy resin/rubber powder/hollow beads three-phase composite specimen shown in Figure 2d becomes larger, and the three-phase composite specimen continues to expand around the specimen under the action of stress. When the strain reaches 50%, the epoxy resin/rubber powder/hollow beads three-phase composite specimen as shown in Figure 2e shows that the fracture occurs under the stress, and the crack expands and extends outward from the center of the three-phase composite specimen. When the strain is 70%, as shown in Figure 2f the fracture zone of the epoxy resin/rubber powder/hollow beads three-phase composite specimen under stress is almost continuous throughout the specimen, and at this time the specimen fails in its ability to absorb energy.

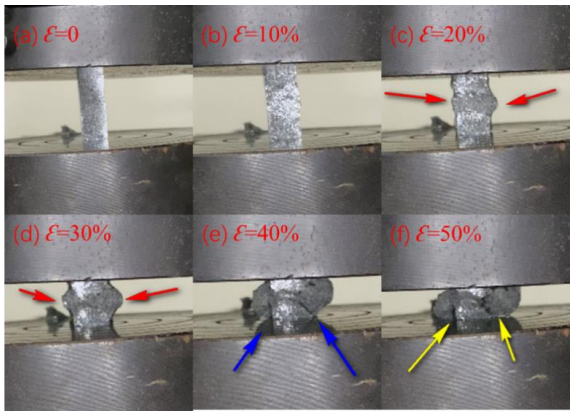

Figure 2. Macroscopic deformation of composites during compression

Figure 3 shows the compressive stress-strain curves of epoxy resin/rubber powder/hollow beads three-phase composite specimen sets containing different mass fractions (5%, 10%, 15%, 20%) of fly ash hollow beads, It can be seen that before the strain reaches 45%, the initial stage of quasi-static compression test is a linear relationship between the stress rises rapidly in the linear-elastic region, this stage of the specimen set of plastic-elastic deformation occurs in this stage of the withdrawal of the external force specimens can be returned to the state before deformation. When the strain reaches 45%, the overall trend of the stress-strain curve of the specimen group with 5% mass fraction of fly ash hollow beads is that the stress continues to increase, and the stress decrease phase after the end of the yield plateau corresponds to a relatively short strain, and then enters the dense reinforcement phase, and the stress rises rapidly with the increase of the strain. While the three specimen groups with fly ash hollow beads mass fraction of 10%, 15%, and 20% all showed a significant stress decrease stage after the slow increase of stress in the yield plateau area, which is the internal pore collapse stage. With the increase of the mass fraction of fly ash hollow beads, the stress of the specimen group decreased more, in which the stress of the specimen group with a fly ash mass fraction of 20% decreased the fastest amplitude, and when the stress was reduced to the lowest point of the stress in the stage of pore collapse zone, the stress decreased by 76.53%.

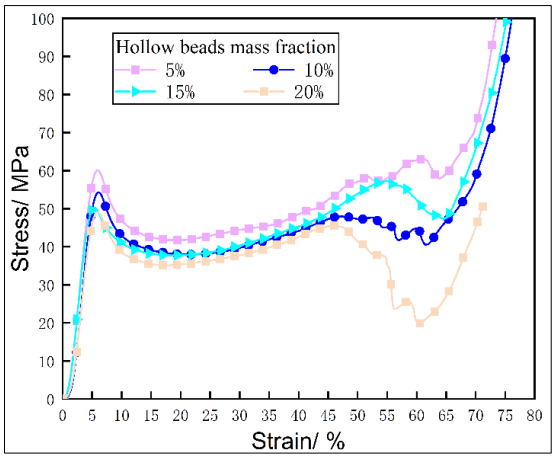

Figure 3. Stress-strain curves of specimens with different mass fractions of hollow beads

With the increase of strain stress, the stresses of the specimen groups with different mass fractions of fly ash hollow beads all reached the collapse point and began to enter the internal collapse stage. Comparing the internal pore collapse stage of specimen groups with different fly ash hollow beads mass fractions, it can be found that the trend of stress-strain curves in the internal pore collapse stage of specimen groups with different fly ash hollow beads mass fractions has a big difference. In order to datum this difference, the following equations 3-6 were used to calculate $\overline{\sigma_p}$, the stress variance in the energy absorption phase of plastic deformation S_p^2, the average stress in the internal pore collapse phase $\overline{\sigma_C}$, and the stress variance in the internal pore collapse phase S_C^2 for the specimen sets with different hollow bead mass fractions:

$$\overline{\sigma_p} = \frac{1}{n}\left(\sigma_{p1} + \sigma_{p2} + \cdots + \sigma_{pn}\right) \tag{3}$$

$$S_p^2 = \frac{\sum_{i=1}^{n}\left(\sigma_1 - \overline{\sigma_p}\right)}{n-1} \tag{4}$$

$$\overline{\sigma_C} = \frac{1}{n}\left(\sigma_{C1} + \sigma_{C2} + \cdots + \sigma_{Cn}\right) \tag{5}$$

$$S_C^2 = \frac{\sum_{i=1}^{n}\left(\sigma_{C1} - \overline{\sigma_{Cn}}\right)}{n-1} \tag{6}$$

$\sigma_{p1} \cdots \sigma_{pn}$ in equation 3 is the value of discrete point stress corresponding to different strains in the energy absorption phase of plastic deformation, $\sigma_{C1} \cdots \sigma_{Cn}$ is the discrete point stress value corresponding to different strains during the internal pore collapse phase, the $\overline{\sigma_p}$ of the plastic deformation energy absorption stage, the stress variance S_p^2 of the plastic deformation energy absorption stage, the average stress $\overline{\sigma_C}$ and of the internal pore collapse stage and and the stress variance S_C^2 of the internal pore collapse stage for the specimen groups with different fly ash hollow beads mass fractions are shown in Table 4 below:

Table 4. Epoxy resin/rubber powder/hollow beads composite material parameter table

Mass fraction of hollow beads	5%	10%	15%	20%
$\overline{\sigma_p}$ **(MPa)**	50.806	43.238	46.575	37.949
S_p^2 **(MPa²)**	33.789	10.953	41.503	50.337
$\overline{\sigma_C}$ **(MPa)**	60.652	45.428	52.372	35.216
S_C^2 **(MPa²)**	3.477	4.590	6.327	68.077

$\overline{\sigma_p}$ of the plastic deformation energy absorption stage of the specimen groups with different fly ash hollow beads mass fractions in the table can characterize the average stress level of the specimens throughout the plastic deformation stage (i.e., the yield plateau stage and the internal pore collapse stage), The stress variance S_p^2 in the energy-absorbing phase of plastic deformation can be used to characterize the degree of stress dispersion of the specimen set in the plastic deformation phase, The average stress $\overline{\sigma_C}$ during the internal pore collapse stage can be used to characterize the average stress level of the specimen during the internal pore collapse stage, The stress variance S_C^2 in the internal pore collapse stage can be used to characterize the degree of stress dispersion in the specimen during the internal pore collapse stage. It can be seen that the specimen group with 10% mass fraction of fly ash hollow beads has the smallest stress variance S_p^2 in the energy-absorbing stage of plastic deformation, and its deformation stability in the plastic deformation stage is the most excellent. The specimen group with 20% mass fraction of fly ash hollow beads had the largest stress variance S_C^2 and the worst deformation resistance stability in the internal pore collapse stage.

Figure 4 shows the comparison of yield strength and compression modulus calculated from the stress points of the stress-strain curves of the epoxy resin/rubber powder/hollow beads three-phase composite specimen set with different mass fractions of fly ash hollow beads added. It can be seen that with the increase of the mass fraction of fly ash hollow beads, the yield strengths of the specimen groups containing different mass fractions of fly ash hollow beads are gradually decreasing. The incorporation of fly ash hollow beads did not improve the stiffness of the epoxy matrix, but rather reduced the stiffness of the epoxy matrix during the initial stage of compression.

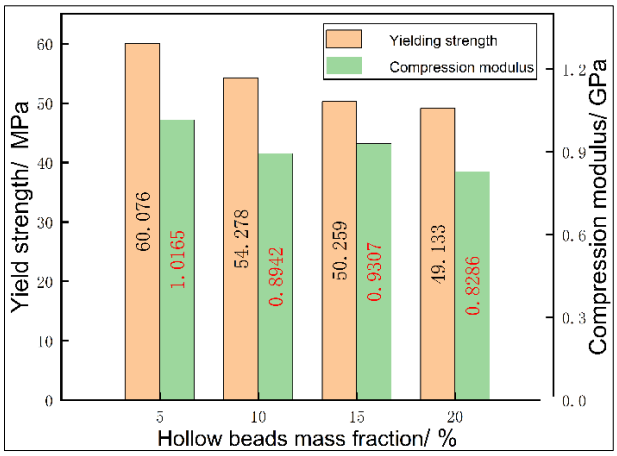

Figure 4. Yield strength and compression modulus of specimens

Figure 5 shows the maximum stress variation range calculated from the stress-strain curves of the epoxy resin/rubber powder/hollow beads three-phase composite specimen set with different mass fractions of fly ash hollow beads added. The maximum stress variation ranges of the specimen groups with 5%, 10%, 15%, and 20% mass fractions of fly ash hollow beads were 18.353 MPa, 16.358 MPa, 12.538 MPa, and 14.039 MPa, respectively. The epoxy resin/rubber powder/hollow beads three-phase composites with fly ash hollow beads mass fractions of 5%, 10%, and 20% showed slightly poorer deformation stability at the initial stage of deformation, while the epoxy resin/rubber powder/hollow beads three-phase composites with added fly ash hollow beads mass fraction of 15% showed much better deformation stability at the initial stage of deformation.

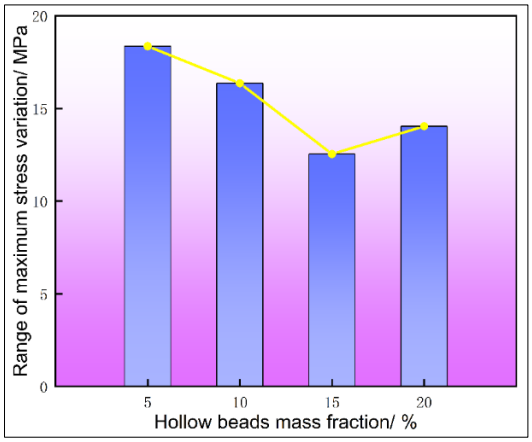

Figure 5. Maximum stress variation range of the specimen

3.3. Analysis of energy absorption properties of materials

The energy absorption capacity E of the epoxy resin/rubber powder/hollow beads three-phase composites can be expressed by equation 7 and the energy absorption efficiency I_E can be expressed by equation 8:

$$E = \int_0^{\varepsilon} \delta \, d\varepsilon \tag{7}$$

$$I_E = \frac{l}{\varepsilon \cdot \sigma_{max}} \int_0^{\varepsilon} \delta \, d\varepsilon \tag{8}$$

In equation 7, ε and σ denote the instantaneous strain and instantaneous stress, respectively, at the corresponding moments in the static compression process. E denotes the energy absorbed by the specimen compressed to the current strain. In equation 8, I_E is the maximum compressive stress that the specimen is subjected to at a strain of $0 \sim \varepsilon$.

Figure 6 shows the energy absorption curves plotted according to equation 7 for different mass fractions of fly ash hollow beads specimen sets. It can be seen that among the group of specimens with different mass fractions of fly ash hollow beads, the highest energy absorption efficiency was achieved with a mass fraction of 5% of fly ash hollow beads, The energy absorption of the specimen groups with different mass fractions of fly ash hollow beads (5%, 10%, 15%, and 20%) was 37.301 MJ/m^{-3}, 33.404 MJ/m^{-3}, 33.883 MJ/m^{-3}, and 31.270 MJ/m^{-3}, respectively, when the strain was 50%.

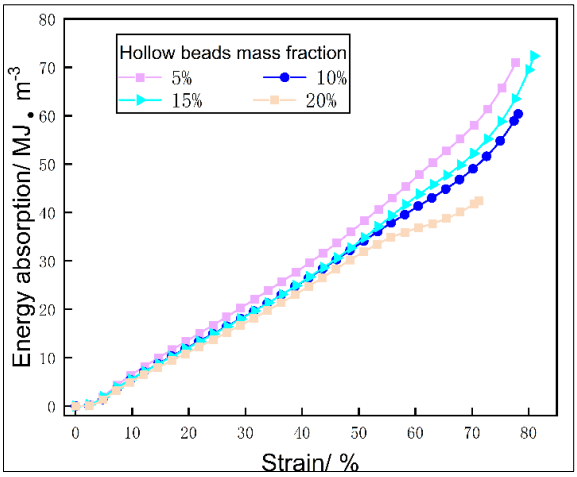

Figure 6. Energy absorption curve of the specimen

Figure 7 shows the energy-absorption efficiency curves of epoxy resin/rubber powder/hollow beads three-phase composite specimen sets with different mass fractions of fly ash hollow beads plotted according to equation 8. It can be seen that the strain corresponding to the plateau region with higher energy absorption efficiency ranges from 10% to 70% throughout the compression-absorption process. The energy absorption efficiency of the specimen group with 15% mass fraction of fly ash hollow beads was overall higher until the strain reached 45%, with the highest energy absorption efficiency of 79.13%. The energy absorption efficiencies of the four specimen groups with different hollow bead mass fractions did not differ much when the strain exceeded 45%. The energy absorption efficiencies of the specimen groups with different mass fractions of fly ash hollow beads (5%, 10%, 15%, and 20%) were 71.25%, 70.78%, 76.67%, and 72.92%, respectively, when the strain was 40%.

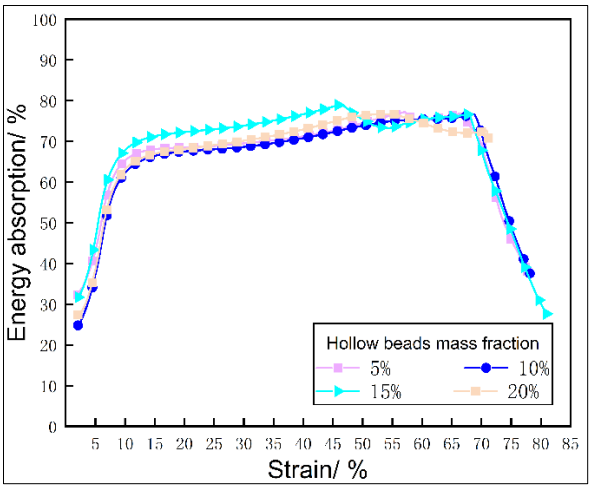

Figure 7. Energy absorption efficiency curve of the specimen

3.4. Analysis of microscopic failure behavior of composite materials

The following are SEM images of epoxy resin/rubber powder/hollow beads three-phase composite specimen sets with different fly ash hollow bead mass fractions (5%, 10%, 15% and, 20%) after quasi-static compression experiments. In the figure, fly ash hollow beads were selected with red boxes, and N220 carbon black rubber powder was selected with yellow boxes. By observing the microscopic morphology of epoxy resin/rubber powder/hollow beads three-phase composites with four different fly ash hollow bead mass fractions, it can be seen that the number of hollow bead compression fragments distributed on the fracture surfaces of the compression specimens of the specimen groups with different hollow bead mass fractions increases with the increase of the fly ash hollow bead mass fraction.

Moreover, by observing the fragments of fly ash hollow beads dislodged around the fracture surfaces and fracture zones, it can be found that the shape and size of the compressed fragments of hollow beads in the compression specimens of the specimen groups with different hollow bead mass fractions decreased with the increase of the mass fraction of fly ash hollow beads. In the SEM images of compressed specimens with 5 and 10% mass fractions of hollow beads, it can be seen that the fragments of hollow beads are still in the form of "chunks", while when the mass fraction of fly ash hollow beads is increased to 20%, it can be seen that the compressed fragments of hollow beads are further crushed in the SEM images of compressed specimens of the specimen set, and most of them are presented in the form of even smaller "chunks" and "powders".

The specimens of the specimen group with 5% mass fraction of fly ash hollow beads did not have a high content of fly ash hollow beads as a whole, and the SEM images of the compressed specimens are shown in Figure 8. The fracture surface of the specimen after compression can be seen on the fly ash hollow beads after the shedding of the occupancy of the cavity left behind, the specimen internal stress folds are mainly "river-like", the fracture zone can be seen inside the distribution of N220 carbon black rubber powder and hollow beads, and the fracture zone can be seen inside the fracture surface of the specimen after compression of the fracture surface. This indicates that N220 carbon black rubber powder and fly ash hollow beads are the stress concentration points inside the epoxy resin/rubber powder/hollow beads three-phase composite.

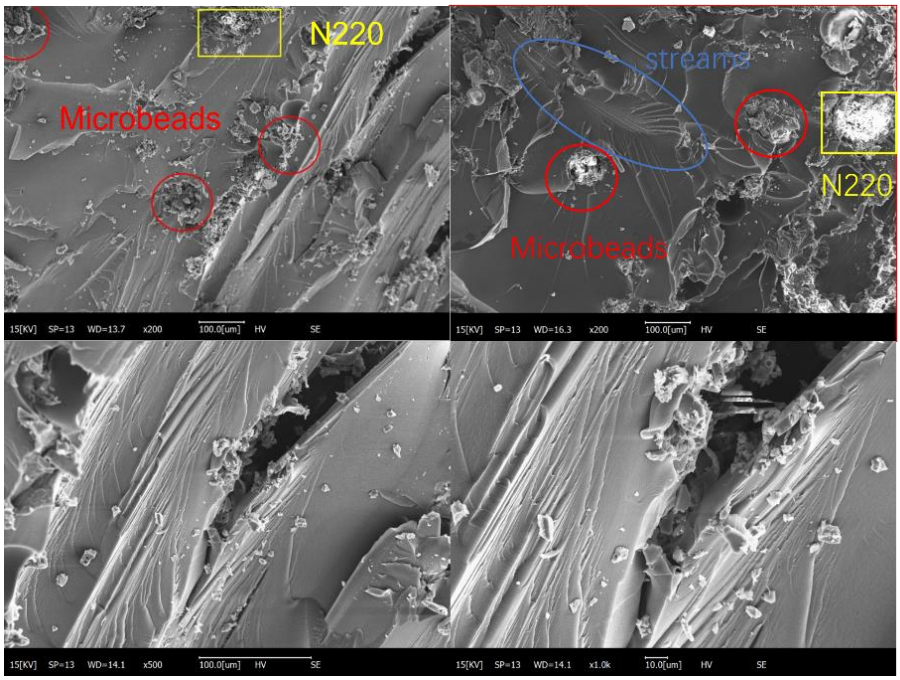

Figure 8. Microscopic morphology of specimens with 5% mass fraction of hollow beads

The SEM image of the compression specimen of the specimen set with 10% mass fraction of fly ash hollow beads is shown in Figure 9. It can be seen that the compression specimen fracture surface dispersed hollow beads compression debris and hollow beads broken off after the occupation of the "cavity" compared with the fly ash hollow beads mass fraction of 5% of the specimen group has increased significantly. These hollow beads break off after the formation of the occupancy of the "cavity" more oval shape, this is because the fly ash hollow beads are crushed under the action of stress, some fragments and epoxy resin matrix peeling off. At this point the formation of the occupied cavity in the compression process continues to be compressed, quasi-static compression experiment after the withdrawal of the external force, the specimen at room temperature in the process of resting will occur during the rebound, the amount of deformation will be returned to part of the. At this time, the

compressed cavity will recover part of the roundness to form an elliptical shape. Some of the occupied cavities still contain compressed fragments of hollow beads, which are present in a "lumpy" form. In the energy absorption stage of plastic deformation, the specimen group with fly ash hollow mass fraction of 10% had more moderate stress changes, smaller range of stress changes, and more stable process of compressive deformation.

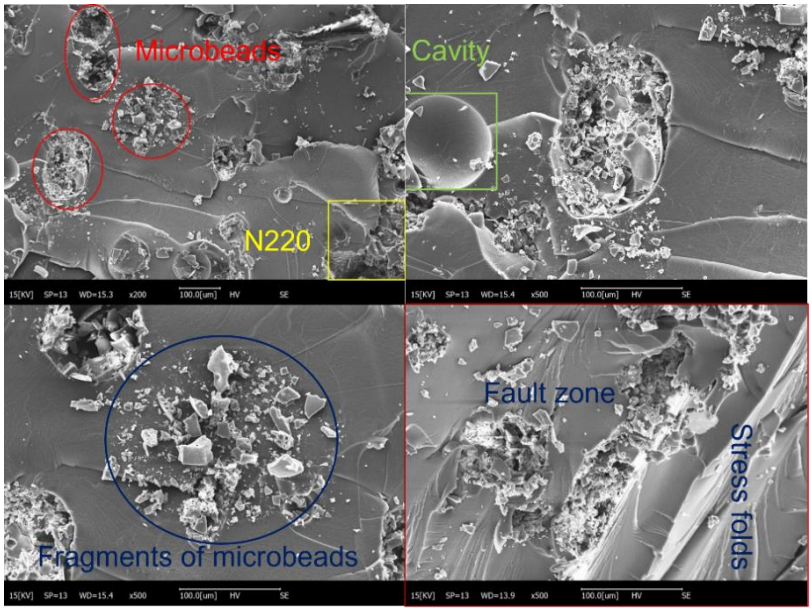

Figure 9. Microscopic morphology of specimens with 10% mass fraction of hollow beads

The SEM image of the compression specimen of the specimen set with 15% mass fraction of fly ash hollow beads is shown in Figure 10. It can be seen that the compression specimen fracture surface scattered hollow beads compression fragments and hollow beads broken off the occupation of the "cavity" compared with the fly ash hollow beads mass fraction of 10% of the specimen group has increased. There are a certain number of occupation cavities distributed at the beginning and termination of the fracture zone, and a part of the occupation cavities are distributed at the turning position of the fracture zone. This suggests that fly ash hollow microbeads can constrain the creation and extension of fracture zones. Combined with Figure 3, the strength of three-phase composites with 15% mass fraction added decreases in the initial stage of deformation, and the stability against deformation improves. The strain curves of the specimen group with 15% mass fraction of fly ash hollow beads witnessed a short stress decrease phase after the stress at the yield plateau had risen to the apex, during which the energy-absorbing effect of the three-phase composites was enhanced.

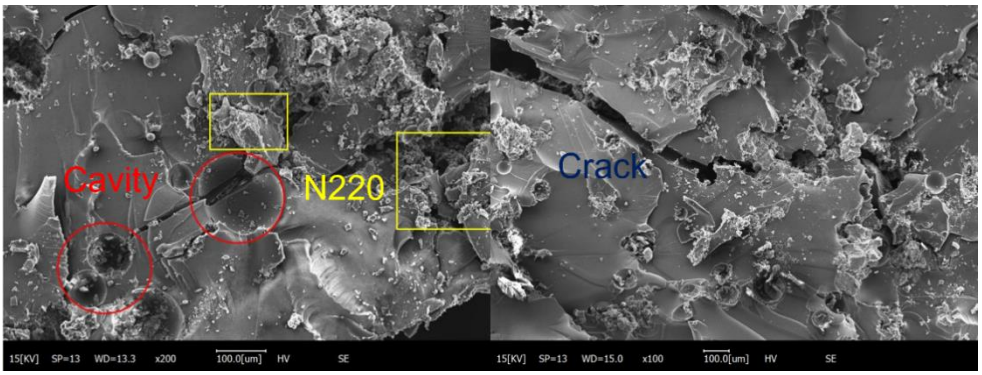

Figure 10. Microscopic morphology of specimens with 15% mass fraction of hollow beads

The SEM image of the compression specimen of the specimen set with 20% mass fraction of fly ash hollow beads is shown in Figure 11. The fracture surfaces and ports of the compression specimens can be seen to be densely populated with compression fragments of smaller hollow beads and "powdered" fragments from further crushing. Compared to the other three specimen sets, the fracture zone of the specimen with 20% mass fraction of fly ash hollow beads was larger after static rebound at room temperature. This is due to the excessive mass fraction of fly ash hollow beads, which severely damaged the internal structure of the epoxy resin/rubber powder two-phase composites. Combined with the stress-strain curves of specimen groups with different hollow bead mass fractions in Figure 3, it can be seen that when the strain exceeds 45%, the fly ash hollow bead mass fraction of 20% specimen group begins to enter the internal pore collapse stage. With the increase of strain, the stress begins to decrease rapidly, and the deformation resistance stability of the specimen with 20% mass fraction of fly ash hollow beads decreases dramatically at this stage compared to the other specimen sets with other mass fractions of fly ash hollow beads.

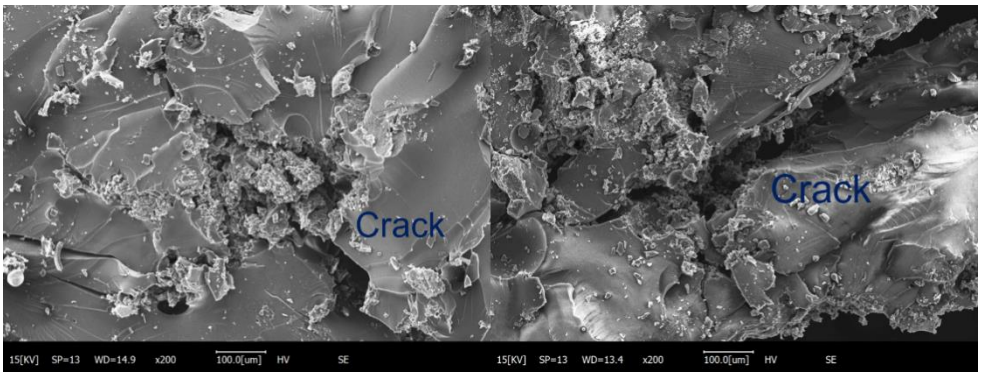

Figure 11. Microscopic morphology of specimens with 20% mass fraction of hollow beads

3.5. Resilience analysis of composites

Specimen groups with different fly ash hollow beads mass fractions were prepared with 10 specimens in each group, and the average length was measured after constant strain compression experiments with one week of natural resting at room temperature, and the resilience was calculated as follows:

$$R = \frac{H_2 - H_1}{H_0 - H_1} \times 100\% \tag{9}$$

Equation (9) where R is the resilience, H_0 is the initial specimen height, H_1 is the specimen height after compression, and H_2 is the specimen height after rebound.

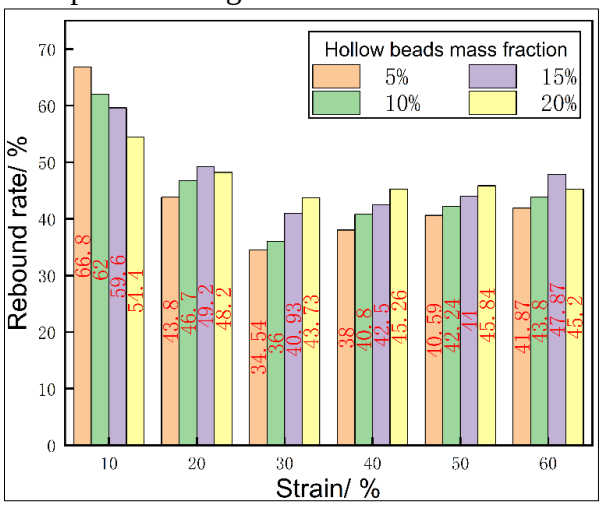

Figure 12. Resilience of specimen groups with different mass fractions of hollow beads

As shown in Figure 12, according to the analysis of the resilience of specimen groups with different mass fractions of fly ash hollow beads, it can be seen that the resilience of specimen groups with the same mass fractions generally shows a decreasing and then increasing trend with the increase of constant strain in the course of fixed-strain quasi-static compression experiments. Among them, the highest resilience was found in the group of specimens with different mass fractions of fly ash hollow beads at 10% constant strain compression. Combined with the stress-strain curves in Figure 3 above, it can be seen that at a strain of 10%, the specimens with different mass fractions pass through the linear elastic zone and the yield point as the stress varies, arriving near the strain corresponding to the trough stress. When the compressive strain of the specimen is the strain corresponding to the linear elastic zone, the specimen is able to return to the initial height if the external force is withdrawn. When the strain reaches 10%, at this time the specimen has just passed the linear elastic zone, the overall compression is small, and the overall performance of the nature of the linear elastic zone. After the quasi-static compression experiments, the rebound amount is larger and the rebound effect is better, so at this time, the rebound rate of specimens with different fly ash hollow beads mass fractions are the highest. At this time, the compression amount is small, the deformation of the specimen is still mainly stress folds, the energy absorption and deformation of the specimen with different mass fractions of fly ash hollow beads is still dominated by the structure of the epoxy resin, so when the specimen is placed at room temperature and rebounded, it is still the rebound amount of the epoxy resin that is the main manifestation. It can be seen that there is a decreasing trend in the resilience of the specimens as the mass fraction of fly ash hollow beads increases at a strain of 10%. When the strain of the constant strain compression experiment is 20%, the compression amount reaches 5 mm, at this time, the rebound recovery nature of the linear elastic region of the specimen is basically destroyed, so the overall rebound rate is greatly reduced compared with the 10% strain constant strain quasi-static compression experiment. It can be seen that at this time the highest resilience was found in the different specimen groups with 15% mass fraction of fly ash hollow beads, and the lowest resilience was found in the specimen group with 5% mass fraction of hollow beads.

The resilience of the epoxy resin/rubber powder/hollow beads three-phase composite specimen group with different mass fractions of fly ash hollow beads added was lower than that of the epoxy resin/rubber powder two-phase composite with 5% mass fraction of N220 carbon black rubber powder when the strains of the constant-strain compression experiments were 30%, 40%, and 50%, respectively. This is because when the strain in the quasi-static compression experiment exceeds 30%, the hollow beads in the epoxy resin/rubber powder/hollow beads three-phase composite specimen set with different mass fractions of fly ash hollow beads added begin to undergo crushing, and absorption of energy under the action of compressive stress, and the occupancy cavities when the hollow beads are intact are formed inside the specimen as shown in Figure 13. Hollow beads in the compression stress under the action of the broken and these in the fracture surface scattered "cavity" in the compression stress can be deformed to absorb energy, improve the energy absorption efficiency of the material, improve the material in the deformation of the energy-absorbing process of the deformation of the stability of the material. In these three strain stages, with the increase of the mass fraction of fly ash hollow beads, the resilience of specimen groups with different fly ash hollow bead mass fractions showed a decreasing trend. This is because, with the increase of the mass fraction of fly ash hollow beads, the number of occupied cavities exposed by the crushing of fly ash hollow beads under the action of compressive stress is also increasing, which leads to the decreasing trend of the resilience of specimen groups with different fly ash hollow bead mass fractions.

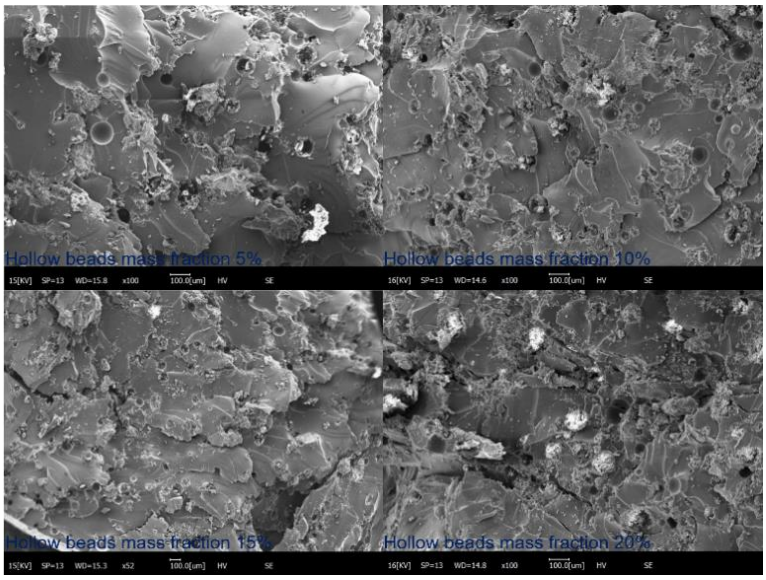

Figure 13. Composite internal cavities

When the strain of the constant strain compression experiment is 70%, the internal pore collapse of the specimen with 20% mass fraction of fly ash hollow beads is too large, which affects the overall stability of the specimen, so when the strain is 70%, the resilience of the specimen group with 20% mass fraction of fly ash hollow beads is lower than that of the specimen group with 15% mass fraction of hollow beads.

3.6. Failure mechanism analysis of composite materials

Combining the mechanical properties of epoxy resin/rubber powder/hollow beads three-phase composites in quasi-static compression experiments and the microstructure morphology at different stages, the failure mechanism of epoxy resin/rubber powder/hollow beads three-phase composites has been analyzed as shown in Figure 14. Initial state of rubber powder particles and hollow beads uniformly distributed in the epoxy resin matrix, the initial state of the center of the fly ash hollow beads is hollow state, the shell contains a certain number of small cavities, the state of the epoxy resin/rubber powder/ hollow beads composite materials for the composite foam structure. With the loading of compression force, the epoxy resin matrix as a whole under the action of compression stress, the matrix undergoes compression deformation, and the middle part of the matrix is the first to undergo expansion deformation. At this stage, the epoxy resin matrix will transfer the compression stress to the uniformly distributed rubber powder particles and hollow beads in the matrix, the rubber powder particles and hollow beads in the compression stress play their own toughness, and deformation to absorb the compression stress, and play the elasticity of the epoxy resin matrix to produce a supporting force, improve the compression of the initial stage of the epoxy resin matrix of the stability of the resistance to deformation. As the compression force continues to act, the strain continues to increase, the compression of the epoxy resin matrix continues to increase, the deformation of the rubber powder and hollow beads inside the matrix also continues to increase, the hollow beads of the shell is crushed, the irregular small cavities in the shell are also deformed under the action of the compression stress, and the fragments are scattered on the fracture surface inside the epoxy resin matrix. Due to the occupancy effect of the hollow beads before crushing, after the hollow beads are crushed, the occupancy "cavity" is exposed inside the epoxy resin matrix, which makes the epoxy resin matrix become a composite foam structure at this stage, and improves the energy-absorbing ability and energy-absorbing efficiency of the epoxy resin/rubber powder/hollow beads composites in the stage of plastic deformation, so that the energy-absorbing efficiency of the three-phase composites in the stage of plastic deformation of the whole material is maintained in the platform at a higher level and improves the stability of the energy-absorbing process, and the absorption of compression stress is more moderate and smooth. The compression force continues

to act, the amount of compression further increases, the epoxy resin composite matrix is further compressed, the deformation of the rubber powder and epoxy resin inside the matrix continues to increase, the hollow microbead fragments are further crushed, and the small irregular cavities inside the shell are compacted.

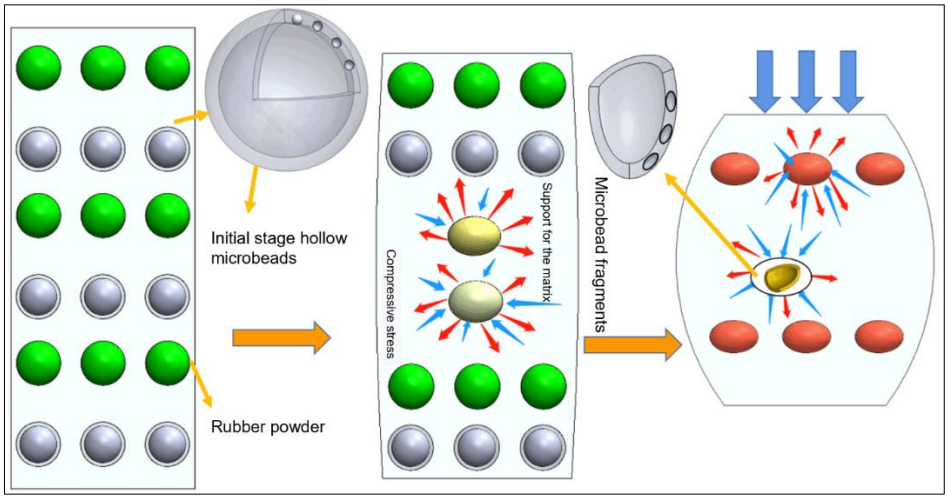

Figure 14. Failure mechanism of epoxy resin/rubber powder/hollow beads composites

In summary, the energy absorption efficiency during the overall compression deformation of epoxy resin/rubber powder/hollow beads composites is high and the change of energy absorption efficiency is small, so the compression deformation process of composites is more stable, and the damage failure mode is more moderate.

4. Conclusions

The epoxy resin/hollow beads/rubber powder three-phase composites with different mass fractions of fly ash hollow beads added to the epoxy resin/rubber powder with a 5% mass fraction of N220 carbon black rubber powder showed a decrease in yield strength during the initial stage of compression, and the mechanical properties in the on-line elastic zone showed even less performance. However, the degree of stress fluctuation in the energy-absorbing phase of plastic deformation is smaller, the deformation stability is better in this phase, the performance of the energy-absorbing buffer is more excellent, and the energy-absorbing efficiency has been greatly improved. Among the different mass fractions of fly ash hollow beads, epoxy resin/hollow beads/rubber powder three-phase composites with a mass fraction of 10% fly ash hollow beads had better mechanical properties, stability during compression deformation, and energy absorption properties.

Acknowledgments: This material is based upon work supported by the Fundamental Research Funds for the Central Universities (grant no. 2572021BC03), Natural Science Foundation of Heilongjiang Province of China (grant no. LH2022C009), the National Key Research and Development Program of China (grant no. 2021YFD220060404), the National Natural Science Foundation of China (grant no. 52371102).

References

1. DU, Y.G., ZHAO, G., SHI, G.H., WANG, Y.M., LI, W., REN, S.T., Effect of crosslink structure on mechanical properties, thermal stability and flame retardancy of natural flavonoid based epoxy resins, *Eur. Polym. J.*, 162, 2022, 8.

2. ZHAO, H.H., LI, J.W., WANG, R., LIU, H.Y., SUN, J.C., WU, J., ZHENG, P.L., An interpenetrating polymer networks structure formed by in situ crosslinking of flame retardant for improvement in mechanical properties and flame retardancy of epoxy resins, *J. Appl. Polym. Sci.*, 140(31), 2023, 15.
3. LAI, G., LIN, S.F., LI, Z.N., ZHANG, H.G., CHEN, M.F., Ladder-like cross-linked network of epoxy resin through multi-site interaction: Flame retardancy and mechanical properties, *J. Appl. Polym. Sci.*, 140(29), 2023, 10.
4. RAMESWARA REDDY, Y., Composite Laminates for Aerospace and Packaging Fields, *Asian Review of Mechanical Engineering*, 12(1), 2023, 39-43.
5. BIFULCO, A., IMPARATO, C., GAAN, S., MALUCELLI, G., ARONNE, A., Hybrid Strategies for the Improvement of the Flame Retardancy of in-situ Silica-Epoxy Nanocomposites cured with Aliphatic Hardener, *Journal of Physics: Conference Series*, 2526(1), 2023, 88-101.
6. RUA, J., BUCHELY, M.F., MONTEIRO, S.N., ECHEVERRI, G.I., COLORADO, H.A., Impact behavior of laminated composites built with fique fibers and epoxy resin: a mechanical analysis using impact and flexural behavior, *J. Mater. Res. Technol-JMRT*, 14, 2021, 428-438.
7. KITICHATPAYAK, D., MAKCHAROEN, W., VITTAYAKORN, N., VITTAYAKORN, W., Influence of various nanofillers on mechanical and electrical properties of epoxy resin composites, *Polym.-Plast. Tech. Mater.*, 61(16), 2022, 1826-1832.
8. XU, W.Z., YAN, H.Y., WANG, G.S., QIN, Z.Q., FAN, L.J., YANG, Y.X., A silica-coated metal-organic framework/graphite-carbon nitride hybrid for improved fire safety of epoxy resins, *Mater. Chem. Phys.*, 258, 2021, 11.
9. MUTHALIF, M.P.A., CHOE, Y., Adhesive and Impact-Peel Strength Improvement of Epoxy Resins Modified with Mono and Diamine Functionalized Elastomers, *Adv. Polym. Technol.*, 202, 2022, 9.
10. SHUNDO, A., AOKI, M., WANG, P.P., HOSHINO, T., YAMAMOTO, S., YAMADA, S., TANAKA, K., Effect of a Heterogeneous Network on the Fracture Behavior of Epoxy Resins, *Macromolecules*, 56(11), 2023, 3884-3890.
11. REMYA, V.P., PARANI, S., SAKHO, E.M., RAJENDRAN, J.V., MALULEKE, R., LEBEPE, T.C., OLUWAFEMI, O.S., Highly Toughened Nanostructured Self-Assembled Epoxy-Based Material-Correlation Study between Nanostructured Morphology and Fracture Toughness-Impact Characteristics, *Polymers*, 15(7), 2023, 12.
12. MISHRA, K., BRASSART, L., SINGH, A., Rate dependent fracture behavior of highly cross-linked epoxy resin, *Eng. Fail. Anal.*, 140, 2022, 12.
13. LI, X.D., WANG, Q., CUI, X., FENG, X.W., TENG, F., XU, M.Y., HE, J., Study on the Mechanical and Toughness Behavior of Epoxy Nano-Composites with Zero-Dimensional and Two-Dimensional Nano-Fillers, *Polymers*, 14(17), 2022, 12.
14. SIENKIEWICZ, N., DOMINIC, M., PARAMESWARANPILLAI, J., Natural Fillers as Potential Modifying Agents for Epoxy Composition: A Review, *Polymers*, 14(2), 2022, 17.
15.SEREKPAYEVA, M., IBZHANOVA, A., NIYAZBEKOVA, R., KOKAYEVA, G., ALDABERGENOVA, S., Properties of Epoxy Resins-Based Composite Materials with the Addition of Microspheres, *Chem. Eng. Technol.*, 46(6), 2023, 1170-1175.
16. KLOSE, L., MEYER-HEYDECKE, N., WONGWATTANARAT, S., CHOW, J., GARCíA, P.P., CARRé, C., LIESE, A., Towards Sustainable Recycling of Epoxy-Based Polymers: Approaches and Challenges of Epoxy Biodegradation, *Polymers*, 15(12), 2023, 23.
17. BALCIOGLU, H.E., Fracture Behaviors of SiC Particle Filled and Jute Fiber Reinforced Natural Composites, *J. Nat. Fibers*, 19(6), 2022, 2338-2355.
18. LIN, J., WANG, K.Q., LI, J.G., YANG, D.S., ZHU, Y.Y., WANG, X.L., Growing metal-organic framework nanoparticles on short carbon fibers to improve flame retardancy, smoke suppression and mechanical properties of the flame retardant epoxy composites, *J. Mater. Sci.*, 56(36), 2021, 19899-19914.

19. OGBONNA, V.E., POPOOLA, A.P.I., POPOOLA, O.M., A review on recent advances on the mechanical and conductivity properties of epoxy nanocomposites for industrial applications, *Polym. Bull.*, 80(4), 2023, 3449-3487.
20. JAYARAMAN, R., KARTHIKEYAN, T., ARUNKUMAR, S., Assessment of compressive and wear performance of waste marble powder and short banana fiber reinforced epoxy composites, *Materials Today: Proceedings*, 91, 2023, 45-57.
21. SHAO, J., ZHU, H., ZUO, X., LEI, W., BORITO, S.M., LIANG, J., DUAN, F., Effect of waste rubber particles on the mechanical performance and deformation properties of epoxy concrete for repair, *Construction and Building Materials*, 241, 2020, 64-78.
22. DEMIR, T.N., YUKSEL YILMAZ, A.N., CELIK BEDELOGLU, A., Investigation of mechanical properties of aluminum–glass fiber-reinforced polyester composite joints bonded with structural epoxy adhesives reinforced with silicon dioxide and graphene oxide particles, *International Journal of Adhesion and Adhesives*, 126, 2023, 57-70.
23. SHI, L.L., SONG, G.J., LI, P.Y., LI, X.R., PAN, D., HUANG, Y.D., GUO, Z.H., Enhancing interfacial performance of epoxy resin composites via in-situ nucleophilic addition polymerization modification of carbon fibers with hyperbranched polyimidazole, *Compos. Sci. Technol.*, 201, 2021, 8.
24. ROSZOWSKA-JAROSZ, M., MASIEWICZ, J., KOSTRZEWA, M., KUCHARCZYK, W., ZUROWSKI, W., KUCINSKA-LIPKA, J., PRZYBYLEK, P., Mechanical Properties of Bio-Composites Based on Epoxy Resin and Nanocellulose Fibres, *Materials*, 14(13), 2021, 16.
25. XU, T., TIAN, J., AN, L.Z., JIAO, Y.M., YIN, Q., TAN, Y.F., Study on the Construction of Dopamine/Poly(ethyleneimine)/Aminoated Carbon Nanotube Multilayer Films on Aramid Fiber Surfaces to Improve the Mechanical Properties of Aramid Fibers/Epoxy Composites, *ACS Omega*, 2022, 16.
26. CHEN, Y., ZHOU, R., WU, D., LIU, Z., SI, Y., LIU, D., XU, R., Boosting interfacial adhesion in PBO fiber/epoxy composite by employing finely granular-structured polyaniline as an interfacial intensifier, *Materials Today Communications*, 35, 2023, 14-26.
27. SARMIN, S.N., JAWAID, M., ISMAIL, A.S., HASHEM, M., FOUAD, H., MIDANI, M., SALIM, N., Effect of chitosan filler on the thermal and viscoelasticity properties of bio-epoxy/date palm fiber composites, *Sustainable Chemistry and Pharmacy*, 36, 2023, 16-32.
28. PERUMAL, K.P.S., BOOPATHI, R., SELVARAJAN, L., VENKATARAMANAN, K., The effects of zircon particles on the mechanical and morphological properties of glass fibre reinforced epoxy composite, *Materials Today Communications*, 37,2023, 12-24.
29. JIANMIN, H., WEI, L., LIFENG, W., YINGCHENG, H., Preparation and Mechanical Properties of Carbon Fiber Reinforced Panel, *Forest Engineering*, 39, 2023, 183-189.
30. WU, Z., WANG, Q.N., ZHAO, S., ZHANG, Y., XUE, B., Study on Mechanical Properties and Fracture Mechanisms of Lignin Fiber/epoxy Resin Composites, *Mater. Plast.*, **60**(1), 2023, 13-24 .
31. SZABó, R., DOLGOS, F., DEBRECZENI, A., MUCSI, G., Characterization of mechanically activated fly ash-based lightweight geopolymer composite prepared with ultrahigh expanded perlite content, *Ceram. Int.*, 48(3), 2022, 4261-4269.
32. BERA, T., PRAKASH, V., ACHARYA, S.K., Erosion wear behaviour of A357/fly ash composites, *Proc. Inst. Mech. Eng. Part J.-J. Eng. Tribol.*, 236(2), 2022, 284-291.
33. WU, Z., JANG, H.F., BO, X., YANG, C.M., ZHANG, Y., WAN, J.Q., Evolution mechanism of compression deformation of carbon black reinforced epoxy resin composites, *Materialwissenschaft und Werkstofftechnik*, 53(10), 2022, 1156-1166.

Manuscript received: 5.11.2023